Computational and Structural Biotechnology Journal 23 (2024) 4161–4176

Contents lists available at ScienceDirect

Computational and Structural Biotechnology Journal

journal homepage: www.elsevier.com/locate/csbj

Research article

Comprehensive gene set enrichment and variation analyses identify *SUV39H1* as a potential prognostic biomarker for glioblastoma immunorelevance

Jixuan Liu [a], Qian Luo [a], Haoran Zhao [a], Mei Yang [a], Jiaying Yang [a], Yingtong Wang [b], Mengxin Zhao [a], Juanjuan Mao [a], Jiasi Chen [a], Baofeng Guo [c,*], Ling Zhang [a,*]

[a] Key Laboratory of Pathobiology, Ministry of Education, Department of Biomedical Science, College of Basic Medical Sciences, Jilin University, Changchun, China
[b] The Undergraduate Center of Hospital of Stomatology, Jilin University, Changchun 130021, China
[c] Department of Plastic Surgery, China-Japan Union Hospital, Jilin University, Changchun 130033, China

ARTICLE INFO

Keywords:
SUV39H1
Glioblastoma
Prognosis
Tumor immunity
GSC

ABSTRACT

Glioblastoma (GBM) is the most common intracranial malignancy. *SUV39H1* encodes a histone H3 lysine 9 methyltransferase that acts as an oncogene in several cancers; however, its role in GBM remains unknown. We obtained GBM transcriptome and clinical data from The Cancer Genome Atlas (TCGA) database on the UCSC Xena platform to perform differential and enrichment analyses of genes in the *SUV39H1* high- and low-expression groups to construct a prognostic risk model. Analysis of *SUV39H1* related biological processes in GBM was performed by gene set enrichment analysis (GSEA) and gene set variation analysis (GSVA). High- and low-risk subgroup mutation signatures were analyzed using maftools. Immune infiltration was evaluated using IOBR and CIBERSORT algorithms. We analyzed the cell types and intercellular communication networks in glioma stem cells (GSCs) using scRNA-seq. The effects on GBM cells and GSCs after inhibition of *SUV39H1* were investigated in vitro. *SUV39H1* was significantly overexpressed in GBM and associated with poor prognosis. *SUV39H1*-related differentially expressed genes were enriched in immune and inflammation related pathways, and GSEA revealed that these genes were significantly enriched in signaling pathways such as IL-18, oxidative phosphorylation, and regulation of TP53 activity. Mutational analysis revealed frequent alterations in TP53 and PTEN expression. In addition, the infiltration abundances of the five immune cell types were significantly different between the high- and low-expression groups. Analysis of cellular communication networks by scRNA-seq revealed a strong interaction between CRYAB-GSC and PTPRZ1-GSC in GSCs. In vitro experiments verified that knockdown of *SUV39H1* inhibited the viability and proliferation of U87 and U251 glioblastoma cells and downregulated the expression of stemness markers Nestin and SOX2 in CSC1589 and TS576 GSC lines. Increased *SUV39H1* expression is associated with immune cell infiltration and poor prognosis in patients with GBM. Inhibition of *SUV39H1* restrains GBM growth and reduces the stem cell properties of GSC. Thus, *SUV39H1* might be a prognostic predictor and immunotherapeutic target in patients with GBM.

1. Introduction

Glioblastoma (GBM) is the most common malignant brain tumor, with an incidence of up to 60 % of cranial tumors. The majority of patients survive for only 12 to 15 months after surgery, with a 5-year survival rate of less than 5 % [1,2]. Currently, the most common treatment for gliomas is surgery, supplemented by radiotherapy and chemotherapy, usually combined with TMZ; however, it also includes molecular-targeted therapy and immunotherapy [3]. Nonetheless, existing mainstream treatments fail to significantly prolong the survival of patients with high-grade gliomas (WHO grade 3–4), and the prognosis of patients remains poor, mainly due to the emergence of tumor recurrence and treatment resistance [4]. Glioma stem cells (GSC), which are considered key factors leading to the formation, maintenance, and

Abbreviations: GBM, glioblastoma; TCGA, The Cancer Genome Atlas; SUV39H1, suppressor of variegation 3–9 homolog 1; GSEA, gene set enrichment analysis; GSVA, gene set variation analysis; GSCs, glioma stem cells.

* Corresponding authors.
E-mail addresses: gbf@jlu.edu.cn (B. Guo), zhangling3@jlu.edu.cn (L. Zhang).

https://doi.org/10.1016/j.csbj.2024.11.016
Received 10 July 2024; Received in revised form 25 October 2024; Accepted 5 November 2024
Available online 6 November 2024

recurrence of gliomas, have the ability to persistently proliferate and promote a high degree of cellular heterogeneity and plasticity within glioblastomas, which in turn causes resistance to radiotherapy and chemotherapy, inducing tumor recurrence [5]. Therefore, it is essential to further explore the mechanisms targeting GBM and GSCs to uncover their key regulators.

In the year 2000, suppressor of variegation 3–9 homolog 1 (*SUV39H1*) was identified as the first human protein lysine methyltransferase [6]. A member of the SUV3–9 family, it contains a SET structural domain that trimethylates lysine 9 of histone H3 (H3K9me3), leading to transcriptional gene silencing [7]. Evidence suggests that *SUV39H1* is highly expressed in tumor tissues and may function as an oncogene. Xin et al. [8] found that chaetocin targets and inhibits *SUV39H1*, suppressing the growth of diffuse endogenous pontine gliomas (DIPG) by down-regulating stemness-related genes and growth factor signaling pathways. Yang et al. [9] found that *SUV39H1* promotes self-renewal and stem cell proliferation of human bladder cancer stem cells through the *SUV39H1*-GATA3-STAT3 pathway. *SUV39H1* also plays a key role in immunotherapy, Lu et al. [10] found that tumor infiltrating cytotoxic T cells (CTLs) in the colon tumor microenvironment have high *SUV39H1* expression, and *SUV39H1* inhibits the expression of CTL effector genes and confers immune escape from colon cancer in the process. A recent study by López-Cobo et al. [11] found that inhibition of *SUV39H1* enhanced the persistence of BBz-CAR T cells, protecting mice from tumor recurrence months after CAR T cell injection. Jain et al. [12] similarly found that early expansion of human-derived CAR T cells, promotion of functional persistence, and overall antitumor efficacy of CD28-based CAR T cells could be enhanced by knockdown of *SUV39H1*. In conclusion, *SUV39H1* is crucial in tumorigenesis, development, and immunotherapy, but its role in GBM is unclear. Further studies are needed to analyze the link between *SUV39H1* and its related gene expression patterns and GBM, as well as the potential mechanism of its action.

Therefore, in this study, we explored the differential expression of *SUV39H1* in gliomas, the associated gene network, their potential functions, and elucidated the possible mechanisms. In addition, the correlation between high- and low-expression *SUV39H1* in GBM, status of immune cell infiltration, and immunotherapy was further investigated. Regarding GSCs, we predicted their key regulators and intercellular communication networks by single-cell sequencing (scRNA-seq) of the GSE dataset. *In vitro* experiments verified the effects of *SUV39H1* inhibition on GBM cell proliferation and stem cell properties of GSCs. In conclusion, this study aimed to determine whether *SUV39H1* is a potential target for glioma treatment.

2. Materials and methods

2.1. Data acquisition and processing

We downloaded GBM-associated RNAseq data in TPM format (n = 1323) from The Cancer Genome Atlas (TCGA) [13] and (GTEx), unified by the Toil process [14] using UCSC Xena (https: //xenabrowser.net/) [15] and analyzed as a test set (TCGA_GTEx- GBM). This test set was analyzed and the corresponding Counts format sequencing and clinical data were obtained through the TCGA official website (https: //portal.gdc.cancer.gov/). The specific clinical information is listed in Table S1. Microsatellite Instability (MSI), Mutation Count, Tumor Mutation Burden (TMB), and fractional genome altered (FGA) scores were obtained from the cBioPortal database [16].

2.2. Differential expression analysis of SUV39H1

Group comparison plots and Receiver Operating Characteristic (ROC) curves of the glioblastoma and normal samples were plotted according to the TCGA_GTEx-GBM dataset. Glioblastoma samples were categorized into *SUV39H1* high-expression and *SUV39H1* low-expression groups based on the median *SUV39H1* expression. Genes in the two groups were differentially analyzed using the R package DESeq2 [17]. The threshold of $|\log FC| > 2$ and adj. $P < 0.05$ was set for differentially expressed genes (DEGs). The results of the analysis of variance were used to plot volcano and heat maps using the R package ggplot2. Functional correlations between DEGs were calculated using the R package GOSemSim [18], and functional correlations between DEGs were analyzed for functional similarity (friends).

2.3. Construction of a prognostic risk model associated with SUV39H1

To construct a prognostic risk model in the glioblastoma dataset (TCGA_GTEx-GBM), we used the R survival package [19] to perform a single multifactorial Cox regression based on *SUV39H1*-associated DEGs to analyze their effect on prognosis. The risk scores were calculated as follows:

$$\text{risk}Score = \sum_{i} Coefficient(gene_i) * mRNA\ Expression(gene_i)$$

The prognostic predictive power of the Cox regression models was demonstrated by KM (Kaplan-Meier) curves and time-dependent ROC. We also constructed clinical prediction models based on the Cox model risk scores for joint age and sex.

2.4. Gene enrichment analysis

Gene Ontology (GO) and Kyoto Encyclopedia of Genes and Genomes (KEGG) enrichment analyses of *SUV39H1*-associated DEGs were performed using the R package clusterProfiler [20]. Gene set enrichment analysis (GSEA) was performed for all genes in the GBM samples from TCGA_GTEx-GBM using the following parameters: seed number 2020, minimum number of genes contained in each gene set 10, and maximum number of genes contained in each gene set, 500. obtained from the Molecular Signatures Database (MSigDB) gene set c2.cp.all.v2022.1. Hs. symbols.gmt [All Canonical Pathways](3050) for GSEA. The screening criteria were adj. $P < 0.05$ and FDR value (q value) < 0.25, with P value correction by Benjamini-Hochberg (BH). The h.all.v7.4.symbols.gmt gene set was obtained from the MSigDB database [21] and gene set variation analysis (GSVA) was performed on all genes of the GBM samples in TCGA_GTEx-GBM to calculate their functional enrichment differences between the two groups (high and low *SUV39H1* expression), the screening criterion was adj. $P < 0.05$.

2.5. Mutational analysis of SUV39H1 high- and low-expression groups

High-frequency mutated genes in patients in the high- and low-risk groups were analyzed using the maftools package [22]. Drug-mutation interactions were analyzed using the Drug Gene Interaction Database (DGIdb). In addition, we performed biological oncogenic pathway analyses of the mutation data to understand which biological oncogenic pathways were affected by the gene mutations.

2.6. Analysis of immune infiltration and differences in immunomodulators

The ESTIMATE immunological and mechanistic scores for GBM samples from TCGA_GTEx-GBM were calculated using the R package IOBR [23]. Comparative grouping plots for the four immune infiltration analyses were constructed using the R package ggplot2.

Immune cell infiltration matrix results were obtained using the CIBERSORT algorithm [24] by combining the LM22 signature gene matrix and filtering the output of data with immune cell enrichment scores greater than zero. The R package ggplot2 was used to paint grouped comparative plots demonstrating the differences in expression in LM22 immune cells between the two groups (high and low *SUV39H1* expression) in GBM samples from TCGA_GTEx-GBM. Subsequently, the

immune cells with significant differences between the two groups were screened for subsequent analyses. Correlations between immune cells were calculated according to the Spearman algorithm and correlation heatmaps were drawn using the R package ggplot2. We also assessed the differential expression of immune checkpoint (ICP) and immunogenic cell death (ICD) regulators in the high and low expression groups.

2.7. Quality control and cellular annotation of single-cell datasets

We used the "CreateSeuratObject" function of the R package Seurat v4.0 [25] to import the Counts matrix of the single-cell (scRNA-seq) dataset GSE128195 and create it as a Seurat object, with the parameter set to have at least 200 gene expression. Cells with $>$ 20 % mitochondrial gene content were excluded. Subsequently, the scRNA-seq dataset GSE128195 was normalized by the "NormalizeData" function. Principal Component Analysis (PCA) was applied to identify the significant principal components (PCs), and the "Elbowplot" function was used to visualize the distribution of P-values. Finally, 15 PCs were selected for Uniform Manifold Approximation and Projection (UMAP) analysis for dimensionality reduction. We use the default parameters of "FindNeighbors" and the 15 PC dimension parameters to construct the K-nearest neighbors of Euclidean distances in the base PCA space. By calling the "FindClusters" function, the "clustree" function is applied to find the resolution of 1.5 to classify the cells into different clusters. The "RunUMAP" function was used for dimensionality reduction to be able to visualize and explore the dataset. Finally, we performed cell type annotation using CellMarker 2.0 (http: //bio-bigdata.hrbmu.edu.cn/CellMarker) [26] on all GBM stem cell cultures from the scRNA-seq dataset GSE128195 to identify the cell types. For the cell taxa that had been annotated, we used the function "FindAllMarkers" to calculate the differential genes between all cell taxa, and screened for differential genes using $|\log2FoldChange| > 0.5$ and P value < 0.05 as the criteria.

2.8. Analysis of glioblastoma stem cell subtypes and cellular communication

The K-nearest neighbors of Euclidean distances in the base PCA space were constructed using the default parameters of "FindNeighbors" and 15 PC dimension parameters. By calling the "FindClusters" function, the "clustree" function is applied to find the resolution of 0.6 to classify the GSCs into different clusters. For different clusters, we used the function "FindAllMarkers" to calculate the differential genes among all cell clusters, and filtered the differential genes with $|\log2FoldChange| > 0.5$ and P Value < 0.05. The gene with the largest log2FoldChange in each cluster was used to define the cell cluster as the new GSC subtype. Cell communication analysis was performed using the R package CellPhoneDB [27].

2.9. Drug resistance analysis of glioblastoma stem cell subtypes

The resistance of each cell subpopulation to different anticancer drugs was predicted using the R package oncoPredict [28] based on drug resistance data from the GDSC [29] database. Drugs with significant differences in drug resistance among the subpopulations were screened and visualized using a combination of box and violin plots.

2.10. Cell Culture

Four cell lines were used in this study: The U87 and U251 cell lines were obtained from the Cell Resource Center of the Shanghai Institutes for Life Sciences. They were cultured in DMEM (Gibco BRL, USA) supplemented with 10 % fetal bovine serum (FBS, Gibco, US). The human glioma stem cell (GSCs) lines TS576 was kindly provided by Cameron Brenner and the Mellinghoff Laboratory at the Memorial Sloan-Kettering Cancer Center (New York, NY, USA). Murine GSCs, CSC1589 waas isolated from *hGFAP-Cre*$^{+}$ *p53*$^{L/L}$ *Pten*$^{L/+}$ mice as previously described [30]. The cells were cultured in neural basal medium (Dulbecco's Modified Eagle's medium/F12, HyClone; GE Healthcare Life Sciences) supplemented with EGF (20 ng/mL) and basic FGF (bFGF; 10 ng/mL). and incubated at 37 °C in a 5 % CO_2 incubator.

2.11. Transfection of siRNA

The cells were transfected using reagents (Thermo Fisher Scientific) according to the manufacturer's protocol. si*SUV39H1* sequences are shown in Table S2. Relevant experiments were performed or cells were collected 48 h after transfection. The siRNA was obtained from GenePharma.

2.12. Cell Counting Kit-8 Assay

Cell viability was assessed after siRNA treatment using a Cell Counting Kit-8 (MedChemExpress) according to the manufacturer's instructions. U87 and U251 cells were inoculated in 96-well plates (100 μl containing 4, 000 cells/well). The cells were transiently transfected after wall attachment and incubated at 37 °C, 5 % CO_2 for 48 h. Then CCK-8 solution (10 μl) was added to the cells for 50–70 min, and the absorbance at 450 nm was detected using an enzyme marker.

2.13. Western Blotting

Cells were lysed with RIPA buffer (containing 1 % protease inhibitor PMSF), total cellular proteins were extracted, and protein samples were separated by SDS-PAGE gel. The proteins were subsequently transferred to PVDF membranes, and the PVDF membranes were closed with 10 % skimmed milk powder for 2 h and incubated with primary antibodies in a refrigerator at 4 °C overnight, using primary antibodies including *SUV39H1* (1:2000; 10574–1-AP; Proteintech Inc.), PCNA (1:5000; 10205–2-AP; Proteintech Inc.), Nestin (1:800; 19483–1-AP; Proteintech Inc.), SOX2 (1:500; 11064–1-AP; Proteintech Inc.), and GAPDH (1:1000; Proteintech Inc.). After washing the membrane, it was incubated with the secondary antibody (1:8000; SA00001–2; Proteintech Inc.) for 1 h. Images of proteins were captured by a chemiluminescence system (BioRad Laboratories). Bands were measured in gray using ImageJ software and statistically analyzed using the GraphPad Prism software.

2.14. EdU-488 Cell Proliferation Assay

According to the manufacturer's instructions (Beyotime), prepare a 2 × EdU working solution by mixing it with culture medium in equal volumes and add it to a 12-well plate, and incubated at 37 °C, 5 % CO_2 for 24 h. Remove the culture medium and add 1 mL of 4 % paraformaldehyde at room temperature to fix the cells for 15 min. The cells were permeabilized with passages containing 0.3 % Triton X-100 for 10–15 min after PBS washing. The click reaction solution was configured and incubated for 30 min away from light, and after PBS washing, the cell nuclei were stained with DAPI for 2 min, and after PBS washing, images were acquired using a BX53 fluorescence microscope (Olympus).

2.15. Immunofluorescence Staining

Cells were fixed with 4 % paraformaldehyde for 20–30 min and permeabilized with 0.3 % Triton X-100 for 10–15 min. After 5 % BSA blocking, the cells were incubated with selected primary antibodies (1:500) at 4 °C overnight. After washing with PBS, the samples were stained with the diluent and then with the corresponding Alexa fluorescence-coupled secondary antibody (1:1000, Invitrogen, Thermo Fisher Scientific, Carlsbad, CA, USA) for 30 min. Treated with DAPI for 2 min and images were acquired using a BX53 fluorescence microscope (Olympus).

2.16. Statistical analysis

R software (version 4.2.2) was used for all statistical analyses of raw letters. The experimental data were statistically analyzed using GraphPad Prism version 9.0. The Wilcoxon rank-sum test was used to compare differences between the two groups. The Kruskal-Wallis test was used to evaluate the differences between the two groups. Correlation analysis was performed using Spearman's correlation method. P value < 0.05 was the threshold for statistical significance.

3. Result

3.1. Differential expression analysis of SUV39H1

To explore the differences in the expression of *SUV39H1* in polyspermatoid glioblastoma and normal samples, we plotted subgroup comparative plots (Fig. 1A) and ROC curves (Fig. 1B) of *SUV39H1* in polyspermatoid glioblastoma and normal samples based on the TCGA_GTEx-GBM dataset. The results showed a significant difference *SUV39H1* in between multiple forming glioblastoma samples and normal samples. We divided the polypoid glioblastoma samples from TCGA_GTEx-GBM dataset into a group with high *SUV39H1* expression and a group with low *SUV39H1* expression. Differential analysis of the TCGA_GTEx-GBM dataset using the R package DESeq2 was performed to obtain the DEGs in the two groups of data, and the results were as follows: there were a total of 19 DEGs in the TCGA_GTEx-GBM dataset that met the threshold of $|\log FC| > 2$ and adj. $P < 0.05$; under this threshold, the number of up-regulated expressed gene totalled 3 (SLC7A3, CAPN6, and OTX2) and down-regulated expressed gene totalled 16 (CCL20, CXCL8, PLA2G2A, PVALB, CCL7, JCHAIN, PI3, DAO, CCL18, KLK7, CXCL6, KLK5, the LCE1C, CSF2, CTAG2, and FDCSP). Volcano plots (Fig. 1C) and heat maps (Fig. 1D) were created based on the results of the variance analysis of this dataset. The genes that played important roles in biological processes (Fig. 1E) were judged by a high or low score of functional similarity (friends) analysis. The results showed that CCL18 was the most important *SUV39H1*-related DEGs.

3.2. Construction of SUV39H1-related prognostic risk model

To construct a prognostic risk model in the glioblastoma dataset

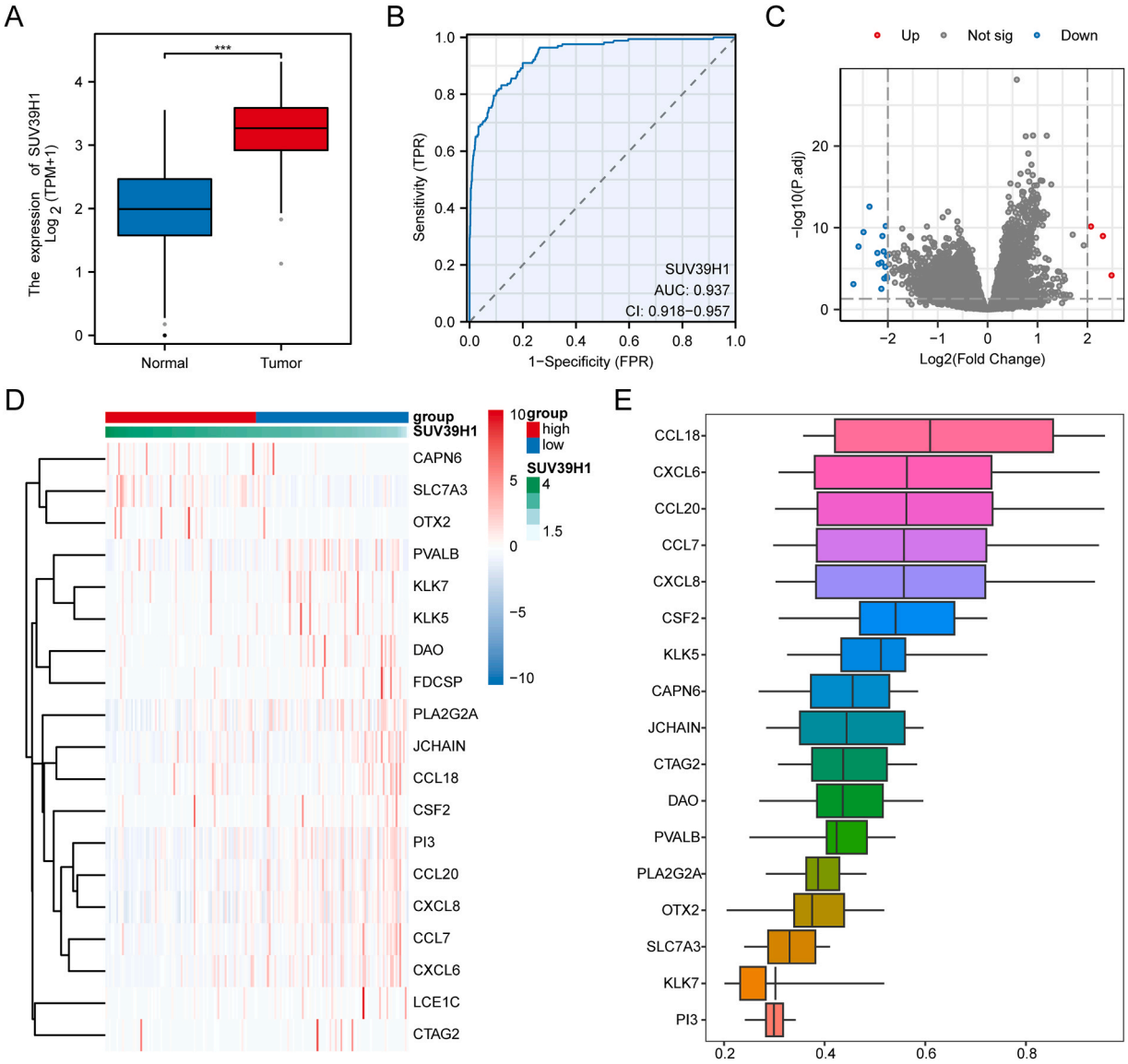

Fig. 1. *SUV39H1* differential expression analysis A-B. Group comparison plots (A) and ROC (B) of *SUV39H1* in the TCGA_GTEx-GBM dataset between glioblastoma and normal samples. C-D. Volcano plot (C) and heat map (D) of the difference analysis between the *SUV39H1* high- and low-expression groups in the TCGA_GTEx-GBM dataset. E. Bar graph of functional similarity analysis of DEGs related to *SUV39H1*. *** represents P value < 0.001, highly statistically significant.

(TCGA_GTEx-GBM), we firstly analyzed the 19 *SUV39H1*-associated DEGs by univariate Cox regression analysis and plotted the forest plots (Fig. 2A), in which CCL20, CCL7, CXCL6, CSF2, FDCSP met the *P* value < 0.05 (Table S3). We included them in the multifactor Cox regression analysis (Table S4) and plotted the KM curve (Fig. 2B) and time-dependent ROC (Fig. 2C). The multifactorial Cox model had a prognostic predictive ability.

Subsequently, we performed a one-way Cox analysis (Fig. 2D) on the

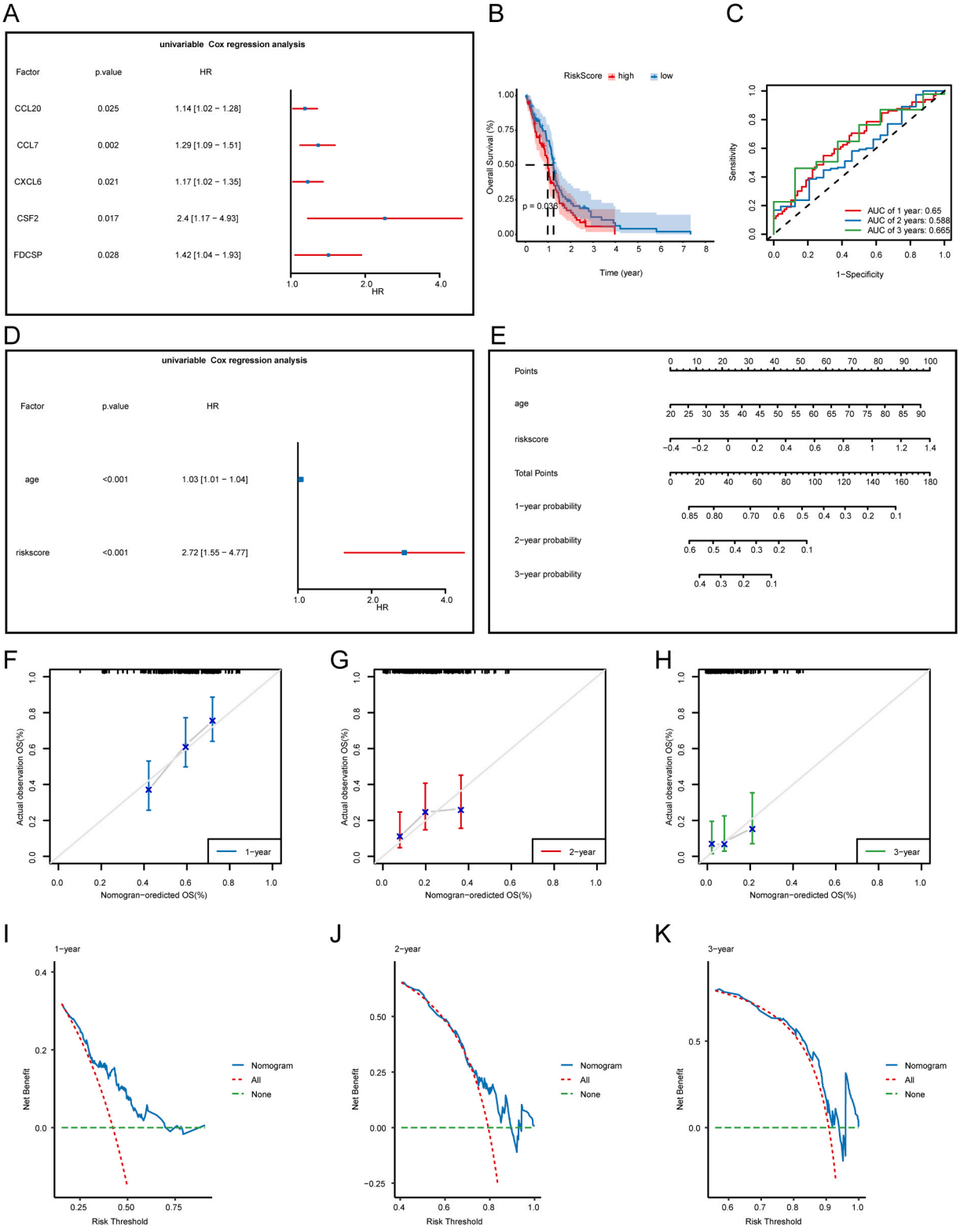

Fig. 2. Construction of *SUV39H1* related prognostic risk model A. *SUV39H1* DEGs related to forest figure Cox, the single factor analysis. B-C. KM curve (B) and time-dependent ROC (C) of the multivariate Cox model for the five *SUV39H1*-related DEGs. D-E. Risk score clinical variables and the single factor of Cox regression analysis of the forest figure (D) and multifactor regression nomogram I. F-H. The calibration curves of clinical prediction models at one year (F), two years (G), and three years (H). Decision curve analysis of clinical prediction models at one year (I), two years (J), and three years (K).

risk score and patient clinical information (gender and age) of the multifactorial Cox model for the five genes (Table S5), and the *P* value of the risk score and age variables were less than 0.05, all of which were included in the multifactorial Cox model (Table S6). We conducted another nomogram analysis to assess the prognostic capacity of the prognostic model (Fig. 2E), and the risk score had a higher utility for the model.

In addition, we performed one year (Fig. 2F), two years (Fig. 2G), and three years (Fig. 2H) The prognostic calibration analyses indicated that the prognostic model we constructed had a better predictive effect.

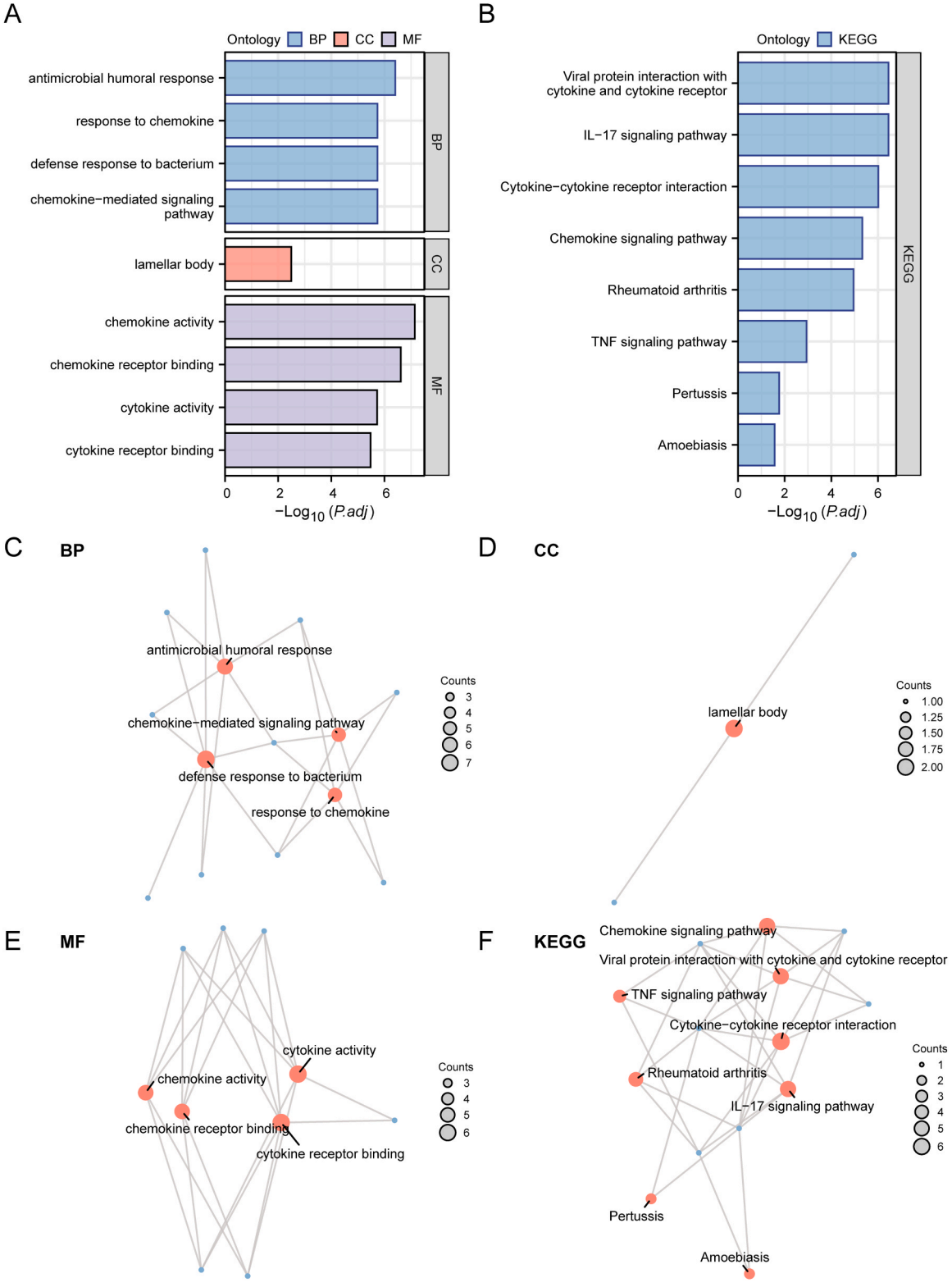

Fig. 3. GO and KEGG enrichment analysis of *SUV39H1*-related DEGs A-B. Bar graph of gene ontology (A) and pathway (B) enrichment analysis results of *SUV39H1*-related DEGs. C-F. Network diagram presentation of biological process (C), cellular component (D), molecular function (E), and biological pathway (F) enrichment analysis results of *SUV39H1*-related DEGs.

We then evaluated the constructed Cox regression prognostic model in terms of clinical utility for one year (Fig. 2I), two years (Fig. 2J), and three years (Fig. 2K) using decision curve analysis (DCA), which showed that our constructed Cox regression prognostic model was clinically predictive for three years > two years > one year.

3.3. Gene ontology (GO) and pathway (KEGG) enrichment analysis

GO and KEGG enrichment analyses found that *SUV39H1*-associated DEGs were enriched in chemokine-mediated signaling pathway, defense response to bacteria, antimicrobial humoral response, response to chemokines, and other biological processes (BP), cellular components such as the lamellar body (CC), and such as cytokine activity, chemokine activity, cytokine receptor binding, and other molecular functions (MF). It was also enriched in the IL-17 signaling pathway, viral protein interaction with cytokines and cytokine receptors, cytokine-cytokine receptor interaction, chemokine signaling pathway, TNF signaling pathway, and other signaling pathways, and the specific results are shown in Table S7. The results of the GO and KEGG enrichment analyses are shown as bar graphs (Fig. 3A, B) and network diagrams (Fig. 3C-F).

3.4. SUV39H1 enrichment of high and low expression genes set analysis (GSEA)

In order to explore the relationship between the expression levels of all genes in the glioblastoma samples and the high and low groups of *SUV39H1* expression,

we performed Gene Set Enrichment Analysis (GSEA) on all genes in the glioblastoma samples, which was demonstrated by a mountain range diagram (Fig 4A), and the results are shown in Table S8. The results showed that all genes in the glioblastoma samples were significantly enriched in WP_IL18_SIGNALING_PATHWAY (Fig 4B), KEGG_OXIDATIVE_PHOSPHORYLATION (Fig 4C), REACTOME_REGULATION_OF_TP53_ACTIVITY (Fig 4D), CTLA4 PID_FOXM1_PATHWAY (Fig 4E) and other biological related functions and signaling pathways.

3.5. Gene set variation analysis of SUV39H1 high and low expression group (GSVA)

GSVA was performed for all genes in the TCGA_GTEx-GBM dataset, and specific information is shown in Table S9. Subsequently, pathways with P values < 0.05, and the differential expression of 20 pathways between the high *SUV39H1* expression group and the low *SUV39H1* expression group were analyzed and visualized using a heatmap (Fig. 5A). Subsequently, validation of differences was performed based on the Mann-Whitney U test, followed by a group comparison plot (Fig. 5B) for the presentation of the results. GSVA results showed that the pathways of inflammatory response, IL6-JAK-STAT3, and unfolded protein response in the *SUV39H1*-expressing high and *SUV39H1*-expressing low groups were statistically significant (P value < 0.05).

3.6. Mutation analysis of SUV39H1 high and low expression group

The R package maftools was used to analyze the mutation characteristics of the high- and low-risk groups, and the results showed that TP53, PTEN, EGFR, TTN, and MUC16 had higher mutation frequencies in the glioblastoma (Fig. 6A). In the results of biological function analysis, the number of genes mutated in RTK−RAS, WNT, NOTCH, Hippo, PI3K and other signaling pathway related genes in the SUV39H1 high expression group was significantly higher than that in the SUV39H1 low expression group, with significant differences (Fig. 6B-C). Next, we

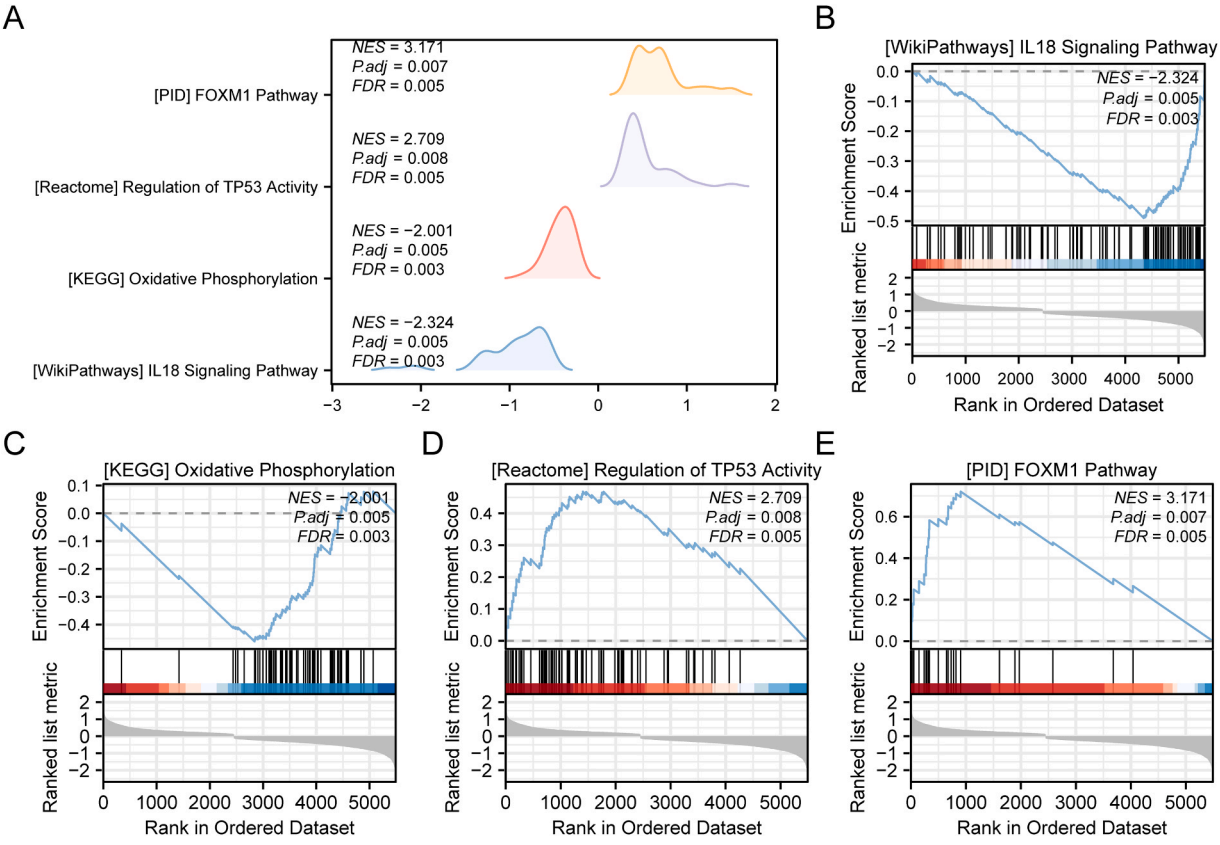

Fig. 4. GSEA of *SUV39H1* high and low expression groups A. GSEA mountain map of 4 biological functions of TCGA_GTEx-GBM dataset. B-E. GSEA showed that the genes in the *SUV39H1* high- and low-expression groups were significantly enriched in WP_IL18_SIGNALING_PATHWAY (B), KEGG_OXIDATIVE_PHOSPHORYLATION (C), REACTOME_REGULATION_OF_TP53_ACTIVITY (D), and CTLA4 PID_FOXM1_PATHWAY (E).

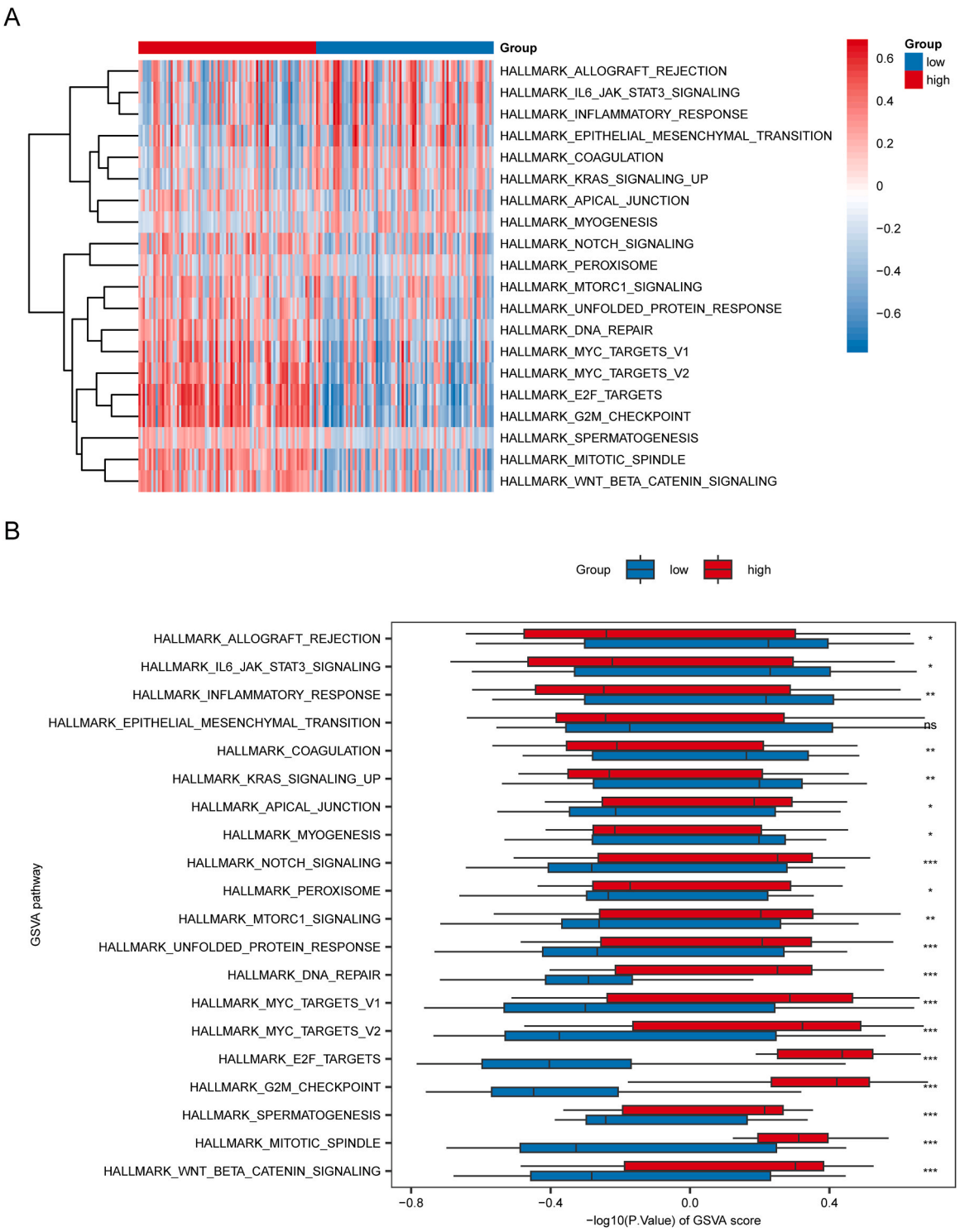

Fig. 5. GSVA of *SUV39H1* high and low expression group A-B. Heatmap (A) and subgroup comparison plot (B) of GSVA results between *SUV39H1* high- and low-expression groups in the TCGA_GTEx-GBM dataset. ns stands for *P* value ≥ 0.05, not statistically significant; * represents *P* value < 0.05, statistically significant; ** represents *P* value < 0.01, highly statistically significant; *** represents *P* value < 0.001 and highly statistically significant.

analyzed the *SUV39H1* high- and low-expression group mutation status, explored genes for medicinal (gene druggability), and the interactions between the drug and gene. Found to predict possible drugs' effects on SUV39H1 high expression of set of genes for DRUGGABLE GENOME [EGFR, GRM3 MUC16, PIK3C2B, PIK3CA] (Fig6D); Predict possible drugs' effects on SUV39H1 lower expression of set of genes for DRUGGABLE GENOME [EGFR, ENPEP; LRP1, MUC16, MUC17] (Fig6E). We analyzed the part of the genome change scores (FGA) (Fig. 6F), Microsatellite Instability (MSI) (Fig. 6G), Mutation Count (Fig. 6H), and Tumor Mutation load (TMB) (Fig. 6I) in *SUV39H1* that showed differences between the high and low expression groups, showing that part of the genome change scores and microsatellite instability in *SUV39H1* were significantly different between the high and low expression groups, and the group showed higher genome change scores and MSI.

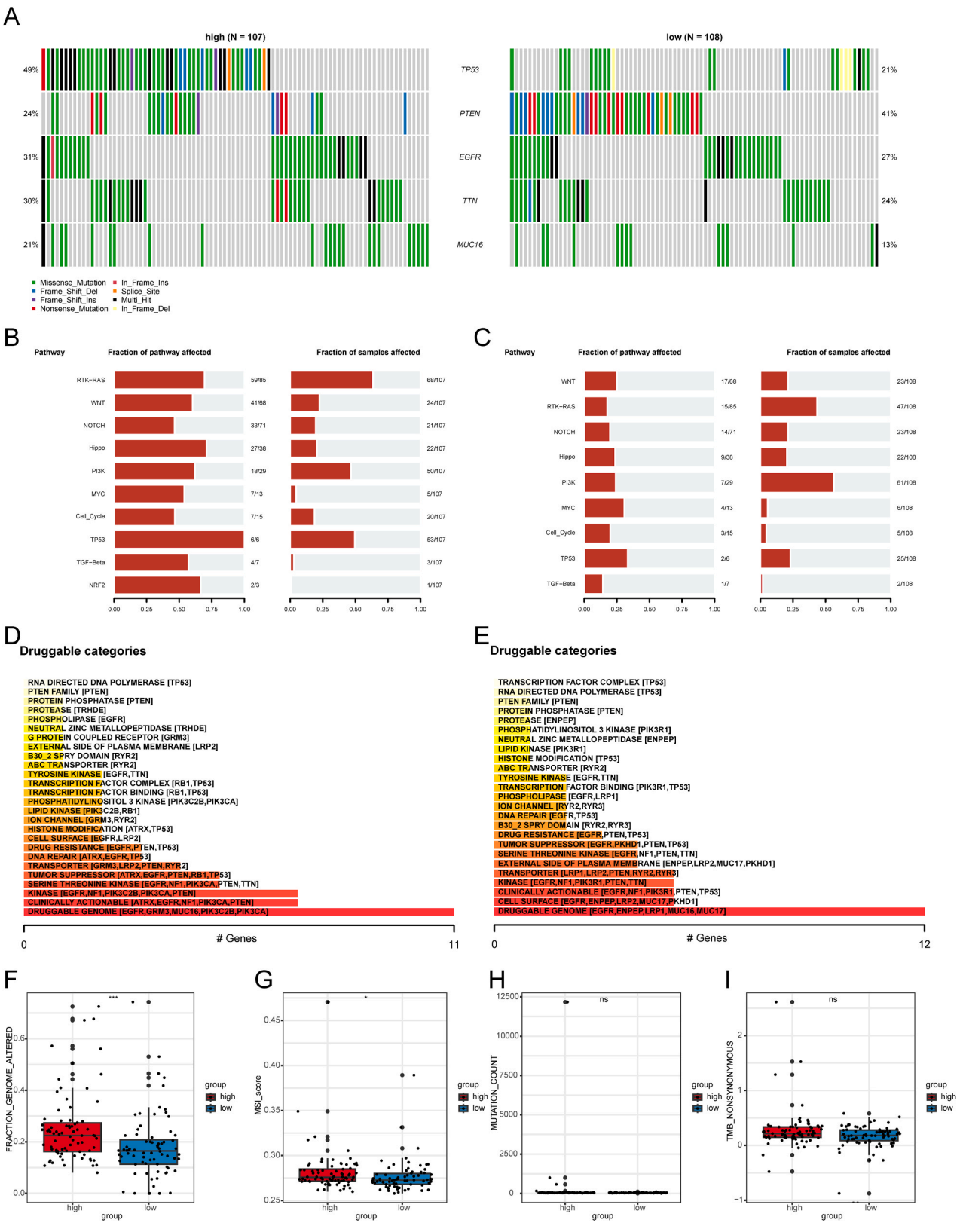

Fig. 6. Mutation analysis of *SUV39H1* high and low expression groups A. Mutant gene landscape of *SUV39H1* high- and low-expression groups. B-C. Analysis of biological functions affected by the mutation in samples from the *SUV39H1* high- (B) and low-expression groups (C). D-E. Classification of potential druggable genes of *SUV39H1* high- (D) and low-expression (E) samples. The top 5 genes are shown in parentheses after each category, and all less than 5 are shown. The X-axis is the number of genes in the patentable gene category. F-I. Riskscore FGA score (F) of high- and low-risk groups, MSI (G), Mutation Count (H), and TMB scores (I) the grouping comparison chart. * represents *P* value < 0.05, statistically significant; ** represents *P* value < 0.01, highly statistically significant; *** represents *P* value < 0.001 and highly statistically significant.

3.7. Immune infiltration of SUV39H1 high and low expression groups

Comparison plots between groups revealed that ESTIMATE score, immune score, stromal scores and tumor purity (Fig. 7A-D) were significantly different between *SUV39H1*-expressing high and *SUV39H1*-expressing low groups ($P < 0.05$).

Stacked bar plots (Fig. 7E) and group comparison plots (Fig. 7F) were used to show the expression differences in the infiltration abundance of immune cells among the different groups. Fig. 7F shows that all five immune cells were statistically significant ($P < 0.05$): naive B cells, memory B cells, monocytes, activated mast cells, and eosinophils. The correlation results of the abundance of the five immune cell infiltrations in the glioblastoma samples are shown in a correlation heat map (Fig. 7G).

3.8. Differential analysis of immunomodulators in high and low SUV39H1 expression groups

Previous studies have indicated that ICPs and ICD regulators play significant roles in modulating host antitumor immunity, which largely influences the efficacy of mRNA vaccines, and that homologous recombination deficiencies are important for immune regulation [31]. Therefore, we assessed the differential expression of ICP and ICD regulators in the *SUV39H1* high- and low-expression groups. The vast majority of ICD regulator genes were significantly upregulated in the *SUV39H1* high expression group (Fig. 7H). Among the ICP regulators, the vast majority of genes were significantly upregulated in the *SUV39H1* low expression group (Fig. 7I). This might predict that patients in the *SUV39H1* high expression group will be more sensitive to immunotherapy, and that the *SUV39H1* low expression group will be more biased towards the immune-tolerant subtype.

3.9. Analysis of cellular communication between stem cell subtypes of glioblastoma

Following the Seurat analysis process, we performed quality control on the single-cell dataset GSE128195 (Fig. 8A). The optimal number of principal components was determined to be 15 by the elbow method (Fig. 8B), and we selected the top 15 principal components for downstream analyses. Twelve cancer cell subpopulations were obtained using unsupervised clustering and were visualized using UMAP (Fig. 8C). We classified all cell clusters into GSCs and no-GSCs by manual annotation (Fig. 8D). Fig. 8E shows the expression of four GSC marker genes, and the expression levels of Nestin and SOX2 were elevated. DEGs among all cellular taxa were calculated using the FindAllMarkers function (Table S10). Fig. S1 shows positive and negative TOP5 expressed genes in GSC and non-GSCs. Fig. 8F shows the expression differences of *SUV39H1*-related DEGs in GSC and no-GSCs, showing that the expression levels of CAPN6, OTX2, and LCE1C were higher in GSC.

To explore the GSC intercellular communication network, the GSC clusters were further clustered to obtain two GSC subtypes and annotated with genes that were significantly differentially expressed, which finally resulted in PTPRZ1-GSCs and CRYAB-GSCs (Fig. 8G). We show the number of interacting receptor ligands between receptor subpopulations in network diagrams (Fig. 8H) and heatmaps (Fig. 8I). The interaction between CRYAB-GSCs and PTPRZ1-GSCs was the strongest among the different subpopulations. This finding suggests a potential functional link between these two cell subtypes that may play a key role in tumor biology. Subsequently, to specifically investigate the ligand interactions between cells, we showed the strength of ligand interactions between different cell subtypes in the form of bubble plots (Fig. 8J); between CRYAB-GSCs and PTPRZ1-GSCs, the PTN-PTPRZ1 ligand pair had a stronger interaction. This interaction may promote cell proliferation, migration, and other tumor-related biological functions. PTPRZ1 as a receptor: In PTPRZ1-GSC, PTPRZ1 activity is regulated by PTN ligands, which may guide the cell signaling process and increase the stemness of tumor stem cells and the aggressiveness of tumors.

3.10. Analysis of drug resistance in glioblastoma stem cell subtypes

Tumor drug resistance has been one of problems urgently to be solved in clinical treatment, in this study, based on the single cell RNA - Seq data, we estimate the two kinds of glioma tumor stem cells for a line of anti-cancer drug resistance, it may be able to provide valuable information for glioma cancer therapy.

Here, drug resistance data from GDSC, glioma cell line expression profiling, and oncoPredict approach were integrated to evaluate the resistance of four first-line anticancer drugs in two cancer cell subsets, gefitinib, ibrutinib, and ibrutinib, respectively. olaparib and temozolomide were also evaluated. The results showed that the drug resistance of the above four drugs in cell subsets was significantly different ($P < 0.05$), specifically, PTPRZ1-GSC was more sensitive to gefitinib (Fig. 8K) and olaparib (Fig. 8M); CRYZB-GSC was more sensitive to ibrutinib (Fig. 8L) and temozolomide (Fig. 8N).

3.11. Quasitime-series analysis of glioblastoma stem cell subtypes

To explore the developmental trajectories of different cell states, we performed a proposed temporal sequence analysis, which demonstrated the developmental trajectories of the five cell states using a differentiation developmental trajectory map (Fig. S2A), a differentiation developmental temporal sequence map (Fig. S2B), and a developmental trajectory map of all cells (Fig. S2C). As shown in Fig. S2D, PTPRZ1-GSC was more predominant in the early stage of cell differentiation and development, and as can be seen from Fig. S2E, the *SUV39H1*-associated DEGs, CAPN6 and LCE1C, were more highly expressed in the late stage of development.

3.12. Knockdown of SUV39H1 inhibits glioma cell proliferation and downregulates stemness markers in GSCs

To investigate the role of *SUV39H1* in gliomas, we inhibited *SUV39H1* expression in U87 and U251 cells using siRNA. CCK8 results showed that cell viability was decreased after inhibition of *SUV39H1* (Fig. 9A). Western blotting results showed that inhibition of *SUV39H1* decreased the levels of Proliferating Cell Nuclear Antigen (PCNA) protein in U87 and U251 cells (Fig. 9B). EdU results similarly demonstrated that inhibition of *SUV39H1* suppressed glioma cell proliferation (Fig. 9C). We further explored the effect of *SUV39H1* inhibition on GSCs and found that the expression of stemness markers Nestin and SOX2 was significantly downregulated in TS576 and CSC1589 cell lines after knockdown of *SUV39H1* treatment by western blotting (Fig. 9D, E) and immunofluorescence staining (Fig. 9F-G). This suggests that *SUV39H1* may be involved in the malignant biological processes of GSC and adversely affect the development of gliomas.

4. Discussion

The current mainstay of treatment for GBM is maximal surgical resection of the tumor. However, the high recurrence rate in patients remains unresolved. Recently, immunotherapy has brought new hope for the treatment of many types of cancer. Immunotherapy for cancer treatment refers to the involvement of the patient's immune system in the recognition and elimination of cancer. Its effectiveness has been demonstrated in a wide range of solid tumor types, including melanoma [32], prostate cancer [33], and bladder cancer [34]. This finding also brings new hope for GBM treatment. Many clinical trials have explored the use of immunotherapy in the context of GBM [35,36]. However, owing to the wide range of immunotherapeutic approaches employed, the different choices of molecular targets, and the diversity of combination therapy strategies, questions regarding the efficacy and safety of immunotherapy for GBM remain. Therefore, novel prognostic targets

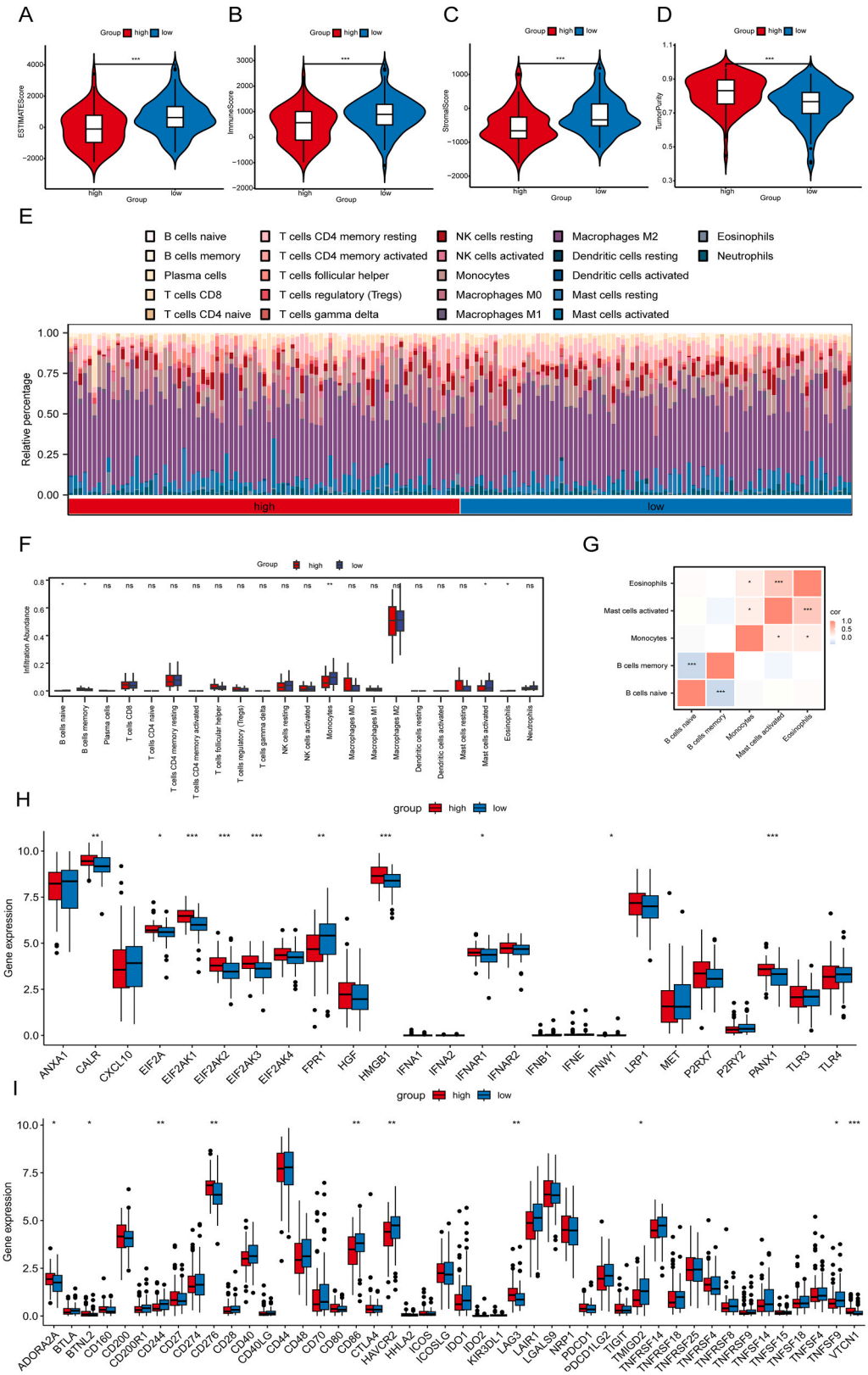

Fig. 7. Immune infiltration of *SUV39H1* high and low expression groups A-D. Group comparison of ESTIMATE (A), immuno (B), stromal (C), and tumor purity (D) scores between *SUV39H1* high- and low-expression groups in glioblastoma samples of the TCGA_GTEx-GBM dataset. E-F. Proportion of LM22 immune cells in the samples of the *SUV39H1* high- and low-expression group (E), as well as comparison group (F). G. The TCGA_GTEx-GBM dataset shows the correlation analysis results of immune cell infiltration abundance in glioblastoma samples. H-I. Group comparison of ICD (H) and ICP (I) modulator expression levels differences between *SUV39H1* high- and low-expression groups. ns stands for P value ≥ 0.05, not statistically significant; * represents P value < 0.05, statistically significant; ** represents P value < 0.01, highly statistically significant; *** represents P value < 0.001 and highly statistically significant.

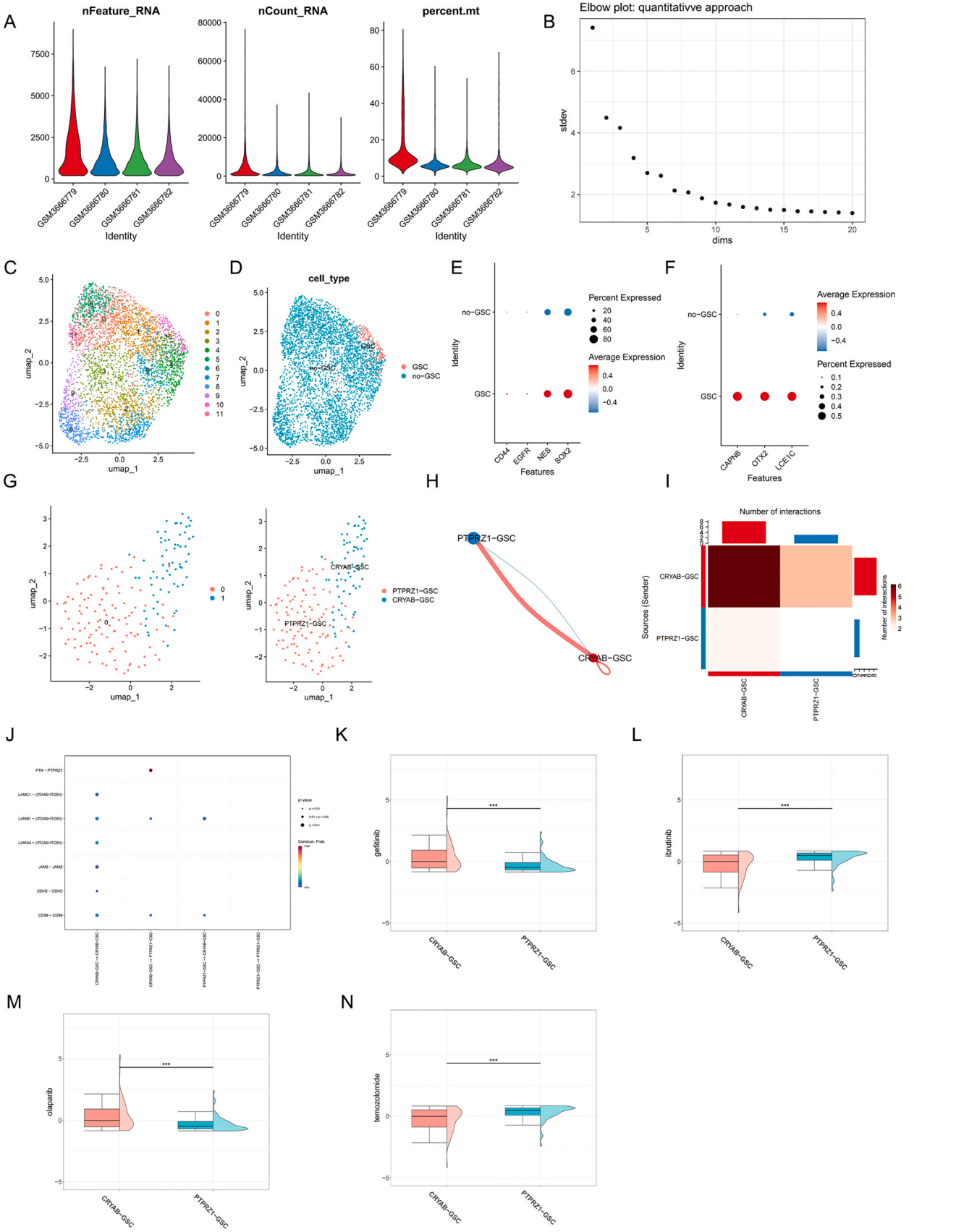

(caption on next page)

Fig. 8. Analysis of cellular communication between GSCs subtypes and drug resistance analysis A. QC nCount_RNA, nFeature_RNA, and mitoRatio violin plots for the GSE128195 single cell dataset. B. Percentage point plots of principal component contribution for the GSE128195 single cell data. C. UMAP clustering plots for cell clusters in the GSE128195 dataset. D. UMAP clustering plots for different cell types in the UMAP clustering plots in the GSE128195 dataset. E. Expression point plots of stem cell marker genes in different cell types. G. UMAP plots of different cell clusters and cell types in the GSC.H-I. Network plots of logarithmic interaction scores between subpopulations of GSCs (H), where different colors represent different cell subpopulations, and the thickness of the lines represent the strength of the interactions and heat maps (I), where the colors from blue to red represent weak to strong interaction strengths, respectively. J. Bubble plots of receptor interactions between GSC subpopulations. K-N. Comparison plots of groupings of drug sensitivity analyses for gefitinib (K), ebrutinib (L), olaparib (M), and temozolomide (N) in different GSC subpopulations. *** stands for P value < 0.001, highly statistically significant.

must be identified.

Aberrant activation or inactivation of enzymes and dysregulation of histone modifications can lead to transcriptional abnormalities in gene expression, and ultimately, the development and progression of gliomas [37]. The H3K9me3 specific histone methyltransferase *SUV39H1* is crucial in epigenetic regulation because it is involved in the composition and regulation of heterochromatin [6]. *SUV39H1* has been implicated in many complex biological processes such as telomere maintenance, cellular differentiation, and senescence [7]. *SUV39H1* was found to be associated with a phenotype of malignant invasion and a high GBM grade compared to normal brain tissue [38]. The *SUV39H1* also plays a key role in tumor immunity, and it has been found that inhibition of *SUV39H1* enhances the anti-tumor immune response, either alone or in combination with anti-PD-1, and is an 'epigenetic checkpoint' for tumor immunity [39]. It is also involved in regulating the survival and proliferation of $CD8^+$ T cells [40]. However, the prognostic significance of *SUV39H1* and the specific mechanisms related to the development and progression of GBM have not been reported yet. Thus, we examined the relationship of SUV39H1 expression to the development of GBM, which could be a potential prognostic biomarker and an immunotherapeutic target for GBM. In addition, the integration of scRNA-seq data further enhances our understanding of the tumor microenvironment and cellular heterogeneity, and this integrated approach is expected to develop more effective diagnostic and therapeutic strategies for patients with GBM.

In this study, we found that *SUV39H1* expression was higher in glioblastoma samples than that in normal samples, and the AUC value of *SUV39H1* in GBM was as high as 0.937, suggesting a high diagnostic value for distinguishing between tumors and normal samples. Next, we divided the GBM samples into *SUV39H1* high-expression and low-expression groups, and identified a total of 19 DEGs, and through the high and low scores of the functional similarity (Friends) analysis, we found that CCL18 was one of the genes with the most significant differences among the *SUV39H1*-related DEGs. Furthermore, CCL18 is a key player in the tumor microenvironment and can influence tumor growth and patient prognosis [41]. These *SUV39H1*-associated DEGs were significantly enriched in biological pathways associated with immune and inflammatory responses by GO and KEGG enrichment analyses, including, but not limited to Interleukin-17 (IL-17), cytokine-cytokine receptor interaction [42], and chemokine signaling pathway [43]. Among them, the IL-17 signaling pathway is crucial in the inflammatory response and has been implicated in the pathogenesis of several cancers [44,45].

In addition, we found that genes in glioblastoma samples were significantly enriched in signaling pathways such as IL-18, oxidative phosphorylation, and regulation of TP53 activity by GSEA. Altered oxidative phosphorylation impairs the immune function of immune cells in the tumor microenvironment, leading to immune escape. *SUV39H1* has been found to be essential in the progression of hepatitis B virus-infected hepatocellular carcinomas and has been identified to target the oxidative phosphorylation pathway [46]. p53 is among the most crucial tumor suppressors and is implicated in the regulation of multiple cancer-related pathways like apoptosis, the cell cycle, inflammatory and immune responses, and DNA damage repair [47]. The encoding gene TP53, which is the most frequently mutated gene in cancers, and the mutation status of TP53 might be a valuable biomarker for predicting the response to cancer immunotherapy in various cancer type [48]. Notably, our analyses revealed that TP53 also has a high mutation frequency in glioblastoma (Fig. 6A). In solid tumors, silencing of TP53 increases *SUV39H1* expression, which induces H3K9me3, leading to chemotherapy resistance [49]. The inhibitory binding of high-affinity IL-18 decoy receptors to mutant IL-18 also promoted NK cell activity, which enhanced antitumor effects in a mouse tumor model [50]. In addition, we identified pathways with significant differences between *SUV39H1* expression groups related to tumor immunity using GSVA, including the signature inflammatory response pathway and the IL-6/JAK/STAT3 signaling pathway. In the tumor microenvironment, IL-6/JAK/STAT3 signaling drives tumor cell proliferation, survival, invasion, and metastasis, while strongly suppressing antitumor immune responses [51]. These findings highlight the potential role of *SUV39H1* in regulating the tumor microenvironment and its involvement in modulating the inflammatory response in the GBM tumor microenvironment.

Our immunoassay results showed significant differences in ESTIMATE algorithm scores (including immune score, stroma score, and tumor purity) between the high *SUV39H1* and low expression groups in glioblastoma, suggesting that *SUV39H1* may influence the composition and immune cell infiltration in the tumor environment. Differences in the infiltration abundance of immune cells in glioblastoma were expressed in the high and low *SUV39H1* expression groups, and we identified the five most statistically significant immune cells as B cells naive, B cells memory, Monocytes, Mast cells activated, and Eosinophils, which Mast cells activated showed a strong positive correlation with Eosinophils. Mast cells (MC) infiltrate mouse and human gliomas in response to various signals in a grade-dependent manner [52]. Eosinophils have also been shown to recruit necrotic tissue in an in vivo mouse model, which is a major determinant of human GBM [53]. The different immune cell compositions and immune scores imply that *SUV39H1* may modulate the immune microenvironment in GBM, which may influence tumor progression and response to immunotherapy, and our results provide a basis for this. ICP and ICD modulators play a crucial role in influencing the efficacy of mRNA vaccines and regulating host antitumor immunity [54,55]. Therefore, we investigated the differential expression of ICP and ICD regulators in high and low *SUV39H1* expression groups. Among them, ICD regulator genes were upregulated in the high *SUV39H1* expression group and ICP regulator genes were upregulated in the low expression group, which may imply that patients with high *SUV39H1* expression may be more sensitive to immunotherapy, whereas patients with low expression may tend to have an immune-tolerant subtype. Overall, our immunological analyses highlighted the importance of *SUV39H1* as a possible immunotherapeutic target for GBM, aiding in the development of new immunotherapeutic strategies.

Current cancer treatment is largely hindered by the presence of cancer stem cells (CSCs). CSCs play a vital role in tumor recurrence and chemoresistance because of their typical stemness characteristics. CSCs protect themselves from immune surveillance by excreting metabolites, cytokines, growth factors, and extracellular vesicles (EVs) into the TME and also regulate the composition of the TME [56]. The high rate of treatment failure in gliomas has been associated with the presence of GSCs, which regain the proliferative capacity of treated tumors and induce tumor recurrence [5], helping tumor cells evade treatment by modulating the composition of the TME and promoting tumor heterogeneity [57]. Therefore, it is necessary to develop new strategies for the

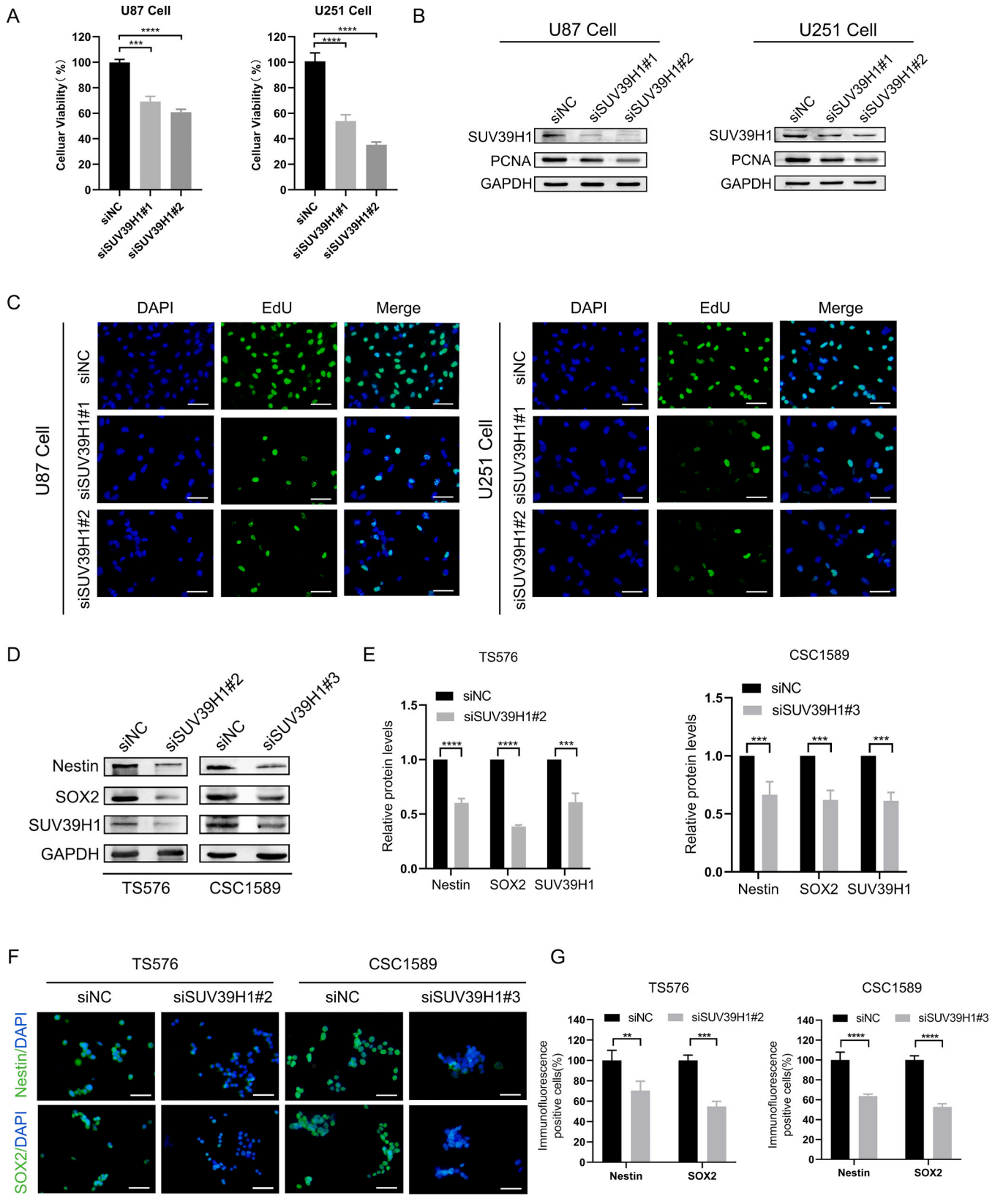

Fig. 9. Knockdown of *SUV39H1* inhibits glioma proliferation and reduces stem cell properties of GSCs A. Viability of U87 and U251 cells tested with the Cell Counting Kit-8 assay after si*SUV39H1* treatment. B. Western blot assay for PCNA expression after knockdown of *SUV39H1*. C. EdU assay for cell proliferation after knockdown of *SUV39H1*. Scale bar: 50 μm. D-E. Western blot analysis showing levels of Nestin and Sox2 after si*SUV39H1* treatment. F-G. Immunofluorescence of Nestin and SOX2 expression in TS576 and CSC1589 cells after 48 h of si*SUV39H1* treatment. Scale bar: 50 μm. *** stands for P value < 0.001, highly statistically significant. **** stands for P value < 0.0001, highly statistically significant.

treatment of GSCs.

We performed scRNA-seq analysis for GSCs and investigated their intercellular communication networks. First, all cell clusters were classified into GSC and non-GSCs, in which the gene expression of the GSC markers Nestin and SOX2 was upregulated. We further clustered the GSC clusters and screened them to obtain two GSC subtypes, annotating them with significantly DEGs, resulting in PTPRZ1-GSCs and CRYAB-GSCs. Protein tyrosine phosphatase, receptor type Z1 (PTPRZ1) is a receptor-like protein tyrosine phosphatase associated with neurodevelopment and known to be overexpressed in glioblastoma [58]. It has been shown that PTPRZ1 interacts with pleiotropic trophic factors secreted by TAMs within GSCs to activate the Akt pathway and maintain the stemness of GSCs [59]. Given its role in cell signaling and interaction with growth factors such as polytrophic factor (PTN) [60], PTPRZ1 might be a key player in the regulation of GSC properties and intercellular communication in the tumor microenvironment. Whereas α-crystallin B chain (CRYAB) is a small heat shock protein expressed mainly in neural and cardiac tissues, and its expression is frequently dysregulated in immune-related diseases [61]. CRYAB expression correlates with tumor-induced immune escape. Upregulation of CRYAB is strongly associated with tumor evasion during immune detection and subsequent immune responses [62]. Knockdown of CRYAB in glioma cells inhibits cell proliferation, migration and induces apoptosis [63]. Cellular communication network analyses indicated that CRYAB-GSCs to PTPRZ1-GSCs had the strongest interactions and might play a role in tumor heterogeneity and progression. Based on the scRNA-Seq data, we estimated the two types of glioma tumor stem cells as a line of anticancer drug resistance, with PTPRZ1-GSCs being more responsive to gefitinib and olaparib, whereas CRYAB-GSCs were more sensitive to ibrutinib and temozolomide. These findings provide valuable information for glioma stem cell therapy.

Finally, we verified by in vitro experiments that knockdown of *SUV39H1* could inhibit the proliferative ability of U87 and U251 cells and found that knockdown of *SUV39H1* significantly downregulated the expression of the GSC surface markers Nestin and Sox2, in GSC1589 and TS576 cells. This evidence suggests that *SUV39H1* might be associated with GSC, being a potential target for GBM due to its crucial role in GSCs.

Despite the comprehensive bioinformatic analyses performed in this study, our study remains limited. First, this study lacks in-depth experimental validation and mechanistic studies on the effect of *SUV39H1* on the efficacy of GBM immunotherapy. Second, the regulatory role of *SUV39H1* in GSCs has not yet been clarified; only the inhibition of *SUV39H1* was found to downregulate the expression of GSC stemness markers, and the specific regulatory mechanisms need to be further explored. Third, the lack of clinical validation analyses indicated that the practical applicability of the risk model in clinical settings remains untested.

5. Conclusions

In conclusion, our study demonstrated that *SUV39H1* expression was higher in glioblastoma samples than that in normal samples, and inhibition of *SUV39H1* suppressed tumor growth. *SUV39H1* was found to be associated with the tumor immune by functional enrichment analysis, mutational profiling, and immune infiltration assessment, indicating the importance of *SUV39H1* as a possible immunotherapeutic target in GBM. Single-cell sequencing analysis further elucidated the heterogeneity of GSC subtypes and intricate cellular communication networks. Furthermore, by targeting GSCs, we found that inhibition of *SUV39H1* significantly downregulated the expression of their stemness markers. Despite these limitations, our findings open a new way of thinking about the future treatment of gliomas.

Funding information

This study was supported by the National Natural Science Foundation of China (Grant No. 82,273,479 to L.Z.), Research Fund of Jilin Provincial Science and Technology Department (20240305079YY to L. Z), China-Japan Union Hospital and College of Basic Medical Sciences, Jilin University Union Project (Grant No. KYXZ2022JC05 to L.Z.), and Jilin University Graduate Student Innovative Research Program Projects (Grant No. 2024CX123 to Jixuan Liu).

CRediT authorship contribution statement

Haoran Zhao: Software, Resources, Data curation. **Qian Luo:** Visualization, Resources, Methodology, Investigation. **Jixuan Liu:** Writing – original draft, Validation, Software, Data curation, Conceptualization. **Ling Zhang:** Writing – review & editing, Writing – original draft, Conceptualization. **Baofeng Guo:** Writing – review & editing, Validation, Supervision, Project administration, Funding acquisition. **Jiasi Chen:** Methodology, Data curation. **Juanjuan Mao:** Methodology, Investigation, Data curation. **Mengxin Zhao:** Methodology, Formal analysis. **Yingtong Wang:** Investigation, Data curation. **Jiayinig Yang:** Software, Investigation, Conceptualization. **Mei Yang:** Software, Investigation, Conceptualization.

Declaration of Competing Interest

All authors declare no conflict of interest.

Appendix A. Supporting information

Supplementary data associated with this article can be found in the online version at doi:10.1016/j.csbj.2024.11.016.

Data Availability

Data are available in a public, open access repository. Data are available on reasonable request. All data relevant to the study are included in the article or uploaded as supplemental information. The datasets (GEO data) and (TCGA-GBM data) for this study can be found in the GEO (https://www.ncbi.nlm.nih.gov/geo/query/acc.cgi?acc=GSE128195) and TCGA (https://www.cancer.gov/about-nci/organization/ccg/research/structural-genomics/tcga).

References

[1] Stupp R, Mason WP, van den Bent MJ, Weller M, Fisher B, Taphoorn MJ, et al. Radiotherapy plus concomitant and adjuvant temozolomide for glioblastoma. N Engl J Med 2005;352(10):987–96.
[2] Sturm D, Bender S, Jones DT, Lichter P, Grill J, Becher O, et al. Paediatric and adult glioblastoma: multiform (epi)genomic culprits emerge. Nat Rev Cancer 2014;14(2):92–107.
[3] Gritsch S, Batchelor TT, Gonzalez Castro LN. Diagnostic, therapeutic, and prognostic implications of the 2021 World Health Organization classification of tumors of the central nervous system. Cancer 2022;128(1):47–58.
[4] Weller M, Wick W, Aldape K, Brada M, Berger M, Pfister SM, et al. Glioma. Nat Rev Dis Prim 2015;1:15017.
[5] Sharifzad F, Ghavami S, Verdi J, Mardpour S, Mollapour Sisakht M, Azizi Z, et al. Glioblastoma cancer stem cell biology: potential theranostic targets. Drug Resist Update: Rev Comment Antimicrob Anticancer Chemother 2019;42:35–45.
[6] Rea S, Eisenhaber F, O'Carroll D, Strahl BD, Sun ZW, Schmid M, et al. Regulation of chromatin structure by site-specific histone H3 methyltransferases. Nature 2000;406(6796):593–9.
[7] Weirich S, Khella MS, Jeltsch A. Structure, activity and function of the Suv39h1 and Suv39h2 protein lysine methyltransferases. Life (Basel, Switz) 2021;11(7).
[8] Xin DE, Liao Y, Rao R, Ogurek S, Sengupta S, Xin M, et al. Chaetocin-mediated SUV39H1 inhibition targets stemness and oncogenic networks of diffuse midline gliomas and synergizes with ONC201. Neuro-Oncol 2024;26(4):735–48.
[9] Yang Z, He L, Lin K, Zhang Y, Deng A, Liang Y, et al. The KMT1A-GATA3-STAT3 circuit is a novel self-renewal signaling of human bladder cancer stem cells. Clin Cancer Res: J Am Assoc Cancer Res 2017;23(21):6673–85.

[10] Lu C, Yang D, Klement JD, Oh IK, Savage NM, Waller JL, et al. SUV39H1 represses the expression of cytotoxic t-lymphocyte effector genes to promote colon tumor immune evasion. Cancer Immunol Res 2019;7(3):414–27.
[11] López-Cobo S, Fuentealba JR, Gueguen P, Bonté PE, Tsalkitzi K, Chacón I, et al. SUV39H1 ablation enhances long-term CAR T function in solid tumors. Cancer Discov 2024;14(1):120–41.
[12] Jain N, Zhao Z, Koche RP, Antelope C, Gozlan Y, Montalbano A, et al. Disruption of SUV39H1-Mediated H3K9 Methylation Sustains CAR T-cell Function. Cancer Discov 2024;14(1):142–57.
[13] Zhang Z, Li H, Jiang S, Li R, Li W, Chen H, et al. A survey and evaluation of Web-based tools/databases for variant analysis of TCGA data. Brief Bioinforma 2019;20 (4):1524–41.
[14] Vivian J, Rao AA, Nothaft FA, Ketchum C, Armstrong J, Novak A, et al. Toil enables reproducible, open source, big biomedical data analyses. Nat Biotechnol 2017;35 (4):314–6.
[15] Goldman MJ, Craft B, Hastie M, Repečka K, McDade F, Kamath A, et al. Visualizing and interpreting cancer genomics data via the Xena platform. Nat Biotechnol 2020; 38(6):675–8.
[16] Gao J, Aksoy BA, Dogrusoz U, Dresdner G, Gross B, Sumer SO, et al. Integrative analysis of complex cancer genomics and clinical profiles using the cBioPortal. Sci Signal 2013;6(269):pl1.
[17] Love MIHW, Anders S. Moderated estimation of fold change and dispersion for RNA-seq data with DESeq2. Genome Biol 2014;15(12):550.
[18] Yu G, Li F, Qin Y, Bo X, Wu Y, Wang S. GOSemSim: an R package for measuring semantic similarity among GO terms and gene products. Bioinformatics 2010;26 (7):976–8.
[19] T T A Package for Survival Analysis in R. R package version 34–0 2022.
[20] Yu G, Wang LG, Han Y, He QY. clusterProfiler: an R package for comparing biological themes among gene clusters. Omics 2012;16(5):284–7.
[21] Liberzon A, Subramanian A, Pinchback R, Thorvaldsdóttir H, Tamayo P, Mesirov JP. Molecular signatures database (MSigDB) 3.0. Bioinformatics 2011;27 (12):1739–40.
[22] Mayakonda A, Lin DC, Assenov Y, Plass C, Koeffler HP. Maftools: efficient and comprehensive analysis of somatic variants in cancer. Genome Res 2018;28(11): 1747–56.
[23] Zeng D, Ye Z, Shen R, Yu G, Wu J, Xiong Y, et al. IOBR: multi-omics immuno-oncology biological research to decode tumor microenvironment and signatures. Front Immunol 2021;12:687975.
[24] Newman AM, Liu CL, Green MR, Gentles AJ, Feng W, Xu Y, et al. Robust enumeration of cell subsets from tissue expression profiles. Nat Methods 2015;12 (5):453–7.
[25] Hao Y, Hao S, Andersen-Nissen E, Mauck WM, 3rd, Zheng S, et al. Integrated analysis of multimodal single-cell data. Cell 2021;184(13):3573–87. e29.
[26] Hu C, Li T, Xu Y, Zhang X, Li F, Bai J, et al. CellMarker 2.0: an updated database of manually curated cell markers in human/mouse and web tools based on scRNA-seq data. Nucleic Acids Res 2023;51(D1):D870–d6.
[27] Efremova M, Vento-Tormo M, Teichmann SA, Vento-Tormo R. CellPhoneDB: inferring cell-cell communication from combined expression of multi-subunit ligand-receptor complexes. Nat Protoc 2020;15(4):1484–506.
[28] Maeser D, Gruener RF, Huang RS. oncoPredict: an R package for predicting in vivo or cancer patient drug response and biomarkers from cell line screening data. Brief Bioinforma 2021;22(6):bbab260.
[29] Yang W, Soares J, Greninger P, Edelman EJ, Lightfoot H, Forbes S, et al. Genomics of Drug Sensitivity in Cancer (GDSC): a resource for therapeutic biomarker discovery in cancer cells. Nucleic Acids Res 2012;41(D1):D955–61.
[30] Zheng H, Ying H, Yan H, Kimmelman AC, Hiller DJ, Chen AJ, et al. p53 and Pten control neural and glioma stem/progenitor cell renewal and differentiation. Nature 2008;455(7216):1129–33.
[31] Shi F, Huang X, Hong Z, Lu N, Huang X, Liu L, et al. Improvement strategy for immune checkpoint blockade: a focus on the combination with immunogenic cell death inducers. Cancer Lett 2023;562:216167.
[32] Ralli M, Botticelli A, Visconti IC, Angeletti D, Fiore M, Marchetti P, et al. Immunotherapy in the treatment of metastatic melanoma: current knowledge and future directions. J Immunol Res 2020;2020:9235638.
[33] Meng L, Yang Y, Mortazavi A, Zhang J. Emerging immunotherapy approaches for treating prostate cancer. Int J Mol Sci 2023;24(18).
[34] Shi R, Wang X, Wu Y, Xu B, Zhao T, Trapp C, et al. APOBEC-mediated mutagenesis is a favorable predictor of prognosis and immunotherapy for bladder cancer patients: evidence from pan-cancer analysis and multiple databases. Theranostics 2022;12(9):4181–99.
[35] Mahmoud AB, Ajina R, Aref S, Darwish M, Alsayb M, Taher M, et al. Advances in immunotherapy for glioblastoma multiforme. Front Immunol 2022;13:944452.
[36] Yu MW, Quail DF. Immunotherapy for glioblastoma: current progress and challenges. Front Immunol 2021;12:676301.
[37] Kunadis E, Lakiotaki E, Korkolopoulou P, Piperi C. Targeting post-translational histone modifying enzymes in glioblastoma. Pharmacol Ther 2021;220:107721.
[38] Spyropoulou A, Gargalionis A, Dalagiorgou G, Adamopoulos C, Papavassiliou KA, Lea RW, et al. Role of histone lysine methyltransferases SUV39H1 and SETDB1 in gliomagenesis: modulation of cell proliferation, migration, and colony formation. Neuromol Med 2014;16(1):70–82.
[39] Niborski LL, Gueguen P, Ye M, Thiolat A, Ramos RN, Caudana P, et al. CD8+T cell responsiveness to anti-PD-1 is epigenetically regulated by Suv39h1 in melanomas. Nat Commun 2022;13(1):3739.
[40] Pace L, Goudot C, Zueva E, Gueguen P, Burgdorf N, Waterfall JJ, et al. The epigenetic control of stemness in CD8(+) T cell fate commitment. Sci (N Y, NY) 2018;359(6372):177–86.
[41] Cardoso AP, Pinto ML, Castro F, Costa ÂM, Marques-Magalhães Â, Canha-Borges A, et al. The immunosuppressive and pro-tumor functions of CCL18 at the tumor microenvironment. Cytokine Growth Factor Rev 2021;60:107–19.
[42] Turhon M, Maimaiti A, Gheyret D, Axier A, Rexiati N, Kadeer K, et al. An immunogenic cell death-related regulators classification patterns and immune microenvironment infiltration characterization in intracranial aneurysm based on machine learning. Front Immunol 2022;13:1001320.
[43] Yi L, Zhou X, Li T, Liu P, Hai L, Tong L, et al. Notch1 signaling pathway promotes invasion, self-renewal and growth of glioma initiating cells via modulating chemokine system CXCL12/CXCR4. J Exp Clin Cancer Res: CR 2019;38(1):339.
[44] Zhang Y, Chandra V, Riquelme Sanchez E, Dutta P, Quesada PR, Rakoski A, et al. Interleukin-17-induced neutrophil extracellular traps mediate resistance to checkpoint blockade in pancreatic cancer. J Exp Med 2020;217(12).
[45] Coffelt SB, Kersten K, Doornebal CW, Weiden J, Vrijland K, Hau CS, et al. IL-17-producing γδ T cells and neutrophils conspire to promote breast cancer metastasis. Nature 2015;522(7556):345–8.
[46] Zhang Y, Lao W, Yang K, Kong X, Li Y, Yu X, et al. SUV39H1 is a novel biomarker targeting oxidative phosphorylation in hepatitis B virus-associated hepatocellular carcinoma. BMC Cancer 2023;23(1):1159.
[47] Kastenhuber ER, Lowe SW. Putting p53 in context. Cell 2017;170(6):1062–78.
[48] Li L, Li M, Wang X. Cancer type-dependent correlations between TP53 mutations and antitumor immunity. DNA Repair 2020;88:102785.
[49] Chiappella A, Diop F, Agostinelli C, Novo M, Nassi L, Evangelista A, et al. Prognostic impact of TP53 mutation in newly diagnosed diffuse large B-cell lymphoma patients treated in the FIL-DLCL04 trial. Br J Haematol 2022;196(5): 1184–93.
[50] Zhou T, Damsky W, Weizman OE, McGeary MK, Hartmann KP, Rosen CE, et al. IL-18BP is a secreted immune checkpoint and barrier to IL-18 immunotherapy. Nature 2020;583(7817):609–14.
[51] Johnson DE, O'Keefe RA, Grandis JR. Targeting the IL-6/JAK/STAT3 signalling axis in cancer. Nat Rev Clin Oncol 2018;15(4):234–48.
[52] Attarha S, Roy A, Westermark B, Tchougounova E. Mast cells modulate proliferation, migration and stemness of glioma cells through downregulation of GSK3β expression and inhibition of STAT3 activation. Cell Signal 2017;37:81–92.
[53] Curran CS, Bertics PJ. Eosinophils in glioblastoma biology. J Neuroinflamm 2012; 9:11.
[54] Dai E, Zhu Z, Wahed S, Qu Z, Storkus WJ, Guo ZS. Epigenetic modulation of antitumor immunity for improved cancer immunotherapy. Mol Cancer 2021;20(1): 171.
[55] Ghouzlani A, Kandoussi S, Tall M, Reddy KP, Rafii S, Badou A. Immune checkpoint inhibitors in human glioma microenvironment. Front Immunol 2021;12:679425.
[56] Wu B, Shi X, Jiang M, Liu H. Cross-talk between cancer stem cells and immune cells: potential therapeutic targets in the tumor immune microenvironment. Mol Cancer 2023;22(1):38.
[57] Eckerdt F, Platanias LC. Emerging role of glioma stem cells in mechanisms of therapy resistance. Cancers 2023;15(13).
[58] He Y, Døssing KBV, Sloth AB, He X, Rossing M, Kjaer A. Quantitative evaluation of stem-like markers of human glioblastoma using single-cell RNA sequencing datasets. Cancers 2023;15(5).
[59] Yang M, Wang B, Yin Y, Ma X, Tang L, Zhang Y, et al. PTN-PTPRZ1 signaling axis blocking mediates tumor microenvironment remodeling for enhanced glioblastoma treatment. J Control Release: J Control Release Soc 2023;353:63–76.
[60] Shi Y, Ping YF, Zhou W, He ZC, Chen C, Bian BS, et al. Tumour-associated macrophages secrete pleiotrophin to promote PTPRZ1 signalling in glioblastoma stem cells for tumour growth. Nat Commun 2017;8:15080.
[61] Thomas OG, Bronge M, Tengvall K, Akpinar B, Nilsson OB, Holmgren E, et al. Cross-reactive EBNA1 immunity targets alpha-crystallin B and is associated with multiple sclerosis. Sci Adv 2023;9(20):eadg3032.
[62] Zhao S, Wang Q, Liu Y, Zhang P, Ji W, Xie J, et al. Interaction, immune infiltration characteristics and prognostic modeling of efferocytosis-related subtypes in glioblastoma. BMC Med Genom 2023;16(1):248.
[63] Cai HB, Zhao MY, Li XH, Li YQ, Yu TH, Wang CZ, et al. Single cell sequencing revealed the mechanism of CRYAB in glioma and its diagnostic and prognostic value. Front Immunol 2023;14:1336187.